Atmos. Meas. Tech. Discuss., 3, 3067–3103, 2010
www.atmos-meas-tech-discuss.net/3/3067/2010/
doi:10.5194/amtd-3-3067-2010
© Author(s) 2010. CC Attribution 3.0 License.

Atmospheric Measurement Techniques Discussions

This discussion paper is/has been under review for the journal Atmospheric Measurement Techniques (AMT). Please refer to the corresponding final paper in AMT if available.

A fully automated FTIR system for remote sensing of greenhouse gases in the tropics

M. C. Geibel, C. Gerbig, and D. G. Feist

Max Planck Institute for Biogeochemistry, Hans-Knöll-Str. 10, 07745 Jena, Germany

Received: 27 June 2010 – Accepted: 7 July 2010 – Published: 22 July 2010

Correspondence to: M. C. Geibel (mgeibel@bgc-jena.mpg.de)

Published by Copernicus Publications on behalf of the European Geosciences Union.

Abstract

This article introduces a new fully automated FTIR system that is part of the Total Carbon Column Observing Network. It will provide continuous ground-based measurements of column-averaged volume mixing ratio for CO_2, CH_4 and several other greenhouse gases in the tropics.

Housed in a 20-foot shipping container it was developed as a transportable system that could be deployed almost anywhere in the world. We describe the automation concept which relies on three autonomous subsystems and their interaction. Crucial components like a sturdy and reliable solar tracker dome are described in detail.

First results of total column measurements at Jena, Germany show that the instrument works well and can provide diurnal as well as seasonal cycle for CO_2. Instrument line shape measurements with an HCl cell suggest that the instrument stays well-aligned over several months.

After a short test campaign for side by side intercomaprison with an existing TCCON instrument in Australia, the system will be transported to its final destination Ascension Island.

1 Introduction

Surface flux estimations of CO_2 on regional to global scales have so far been derived by a combination of data from a global network of surface sites (GLOBALVIEW-CO2, 2009) and the results of global transport models (Gurney et al., 2002; Rayner et al., 1999; Tans et al., 1990). The main advantages of the surface measurements are that they are highly accurate and that they can be obtained with moderate effort even in remote locations. The main disadvantages are that they are stronlgy influenced by local sources and sinks and that they can only provide measurements from within the atmospheric boundary layer. Despite the high accuracy of the measurements themselves, imperfect representation of vertical mixing near the surface in atmospheric transport

AMTD
3, 3067–3103, 2010

models still leads to large uncertainties in modelled tracer mixing ratios (Gerbig et al., 2008).

The existing in situ network can be complemented by precise and accurate total-column-averaged CO_2 volume mixing ratio (VMR) measurements – commonly referred to as xCO_2. The column integral of the CO_2 VMR profile is less sensitive to diurnal variations in atmospheric boundary layer height and details of vertical transport in general (Gerbig et al., 2008). It exhibits less spatial and temporal variability than near-surface in situ data, while retaining information about surface fluxes (Gloor et al., 2000). Rayner and O'Brien (2001) have shown that globally distributed xCO_2 measurements with an accuracy in the range of ±1.5–2.5 ppmv would be effective in constraining global-scale carbon budgets. However, such xCO_2 measurements are still very sparse.

Recent analyses of solar spectra obtained by near-infrared Fourier Transform Spectrometers (FTIR) demonstrate that xCO_2 can be retrieved with high precision (Washenfelder et al., 2006; Warneke et al., 2005; Dufour et al., 2004; Yang et al., 2002). These measurements make use of characteristic absorption lines that many atmospheric trace gases exhibit in the infrared region of the electromagnetic spectrum. From the difference of the known solar spectrum from space and the measured solar spectrum after passing through the atmosphere, the total column of gases like CO_2, CH_4 and many others can be calculated. To obtain the column-averaged volume mixing ratio, these values have to be related either to surface pressure or measured O_2 total column. Unlike surface measurements, the total column measurements provided by ground-based FTIR instruments can also be used directly for the validation of satellite instruments like GOSAT (Yokota et al., 2009).

The Atmospheric Remote Sensing group (ARS) of the Max Planck Institute for Biogeochemistry (MPI-BGC) in Jena, Germany, is currently making the final preparations for installing such an FTIR instrument in the tropics, where such measurements have only been taken within short campaigns (Petersen et al., 2010). The instrument will be part of the Total Carbon Column Observation Network (TCCON) (Toon et al., 2009) that will provide ground-truth data for satellite validation. It will be installed on Ascension

AMTD
3, 3067–3103, 2010

Island, a British oversea territory in the South Atlantic. This unique location should provide excellent observation conditions for the FTIR instrument. Due to its small size and very scarce vegetation, the influence from local sources and sinks on the CO_2 and CH_4 measurements should be minimal.

The instrument has been set up and tested at the MPI-BGC in Jena, Germany. This article provides a technical overview of the system and shows first results obtained during this initial phase.

2 The MPI-BGC FTIR system

Most of the existing FTIR systems are operated either by a person physically sitting next to the instrument or controlled remotely through a data connection. Furthermore, those systems were usually built for one special location and designed to cope with that location's typical special environmental conditions. In contrast to this the main goal of the MPI-BGC's FTIR project was to build an instrument that could be deployed nearly anywhere in the world (Fig. 1).

However, building such a system is challenging. In a remote region with little infrastructure to rely on such an instrument has to be able to run fully automatic without operator intervention for months or even years. This challenge added several problems that had to be solved in addition to setting up the instrument itself. All components had to be designed or modified to minimize the risk of technical failures or software errors. Wherever possible, key devices were simplified to avoid problems arising from unnecessary complexity. Essential devices were set up redundantly to provide essential functions even in the case of a failure.

The components have been chosen on the basis of reliability, stability and maintainability. All of them are grouped into three autonomous modules – each of them designed to perform special tasks in the system as reliably as possible in the most simple way. These modules are the weather station, the Programmable Logic Controller (PLC) and the Master PC. A star-shaped automation concept where all components

AMTD
3, 3067–3103, 2010

are controlled by a single master system would also have created a potential single point of failure. Therefore the three autonomous modules were set up so that they are able to check each other's performance or even reset each other in the case of a failure. Detailed information can be found in Sect. 2.4.

2.1 The container

One of the main targets was to create a system that is relatively easy to transport. Therefore, the system is housed in a custom-made 20-foot shipping container (see Fig. 2). Due to its enhanced insulation and the built-in air conditioning system the container provides stable indoor operating conditions at outdoor temperatures from −40 °C to +40 °C.

The container is fully certified for land as well as ship transport and can be transported like any standard freight container. This offers high flexibility at reasonable shipping prizes.

Besides stable inside environmental conditions, stable electric power is essential for operation. An uninterruptible power supply (UPS) is integrated to bridge power failures of up to two hours.

2.2 Fourier Transform Infrared Spectrometer (FTIR)

The atmospheric measurements are performed by a Bruker 125HR FTIR instrument. The instrument provides high resolution solar absorption spectra over a large spectral range. The resolution of the instrument is 0.0035 cm^{-1} and it covers a bandwidth from 3800 to 15 800 cm^{-1}. Similar to the Park Falls instrument (Washenfelder et al., 2006) it is equipped with two detectors measuring simultaneously in different spectral areas. A silicon diode detector covers the spectral area from 15 800 to 9000 cm^{-1}. A Indium-Gallium-Arsenide (InGaAs) detector covers the spectral area from 12 000 to 3800 cm^{-1}.

AMTD
3, 3067–3103, 2010

To enhance the temperature stability of the system all measurements are performed under vacuum. Therefore the system is equipped with a multi-stage oil-free scroll pump. To avoid vibrations of the pump influencing the measurements, the pump only runs during night time.

For accurate measurements the monitoring of the instrumental line shape is necessary. This is realized as described by Hase et al. (1999) by integrating an HCl gas cell in the beam path inside the FTIR instrument. First results of this procedure are described Sect. 3.1.

The atmospheric measurements are performed with a 0.014 cm^{-1} resolution and two scans (one forward, one backward) per measurement.

2.3 Solar tracker and protective devices

Remote sensing of greenhouse gases via FTIR uses the sun as a light source. The container has an open flange in the roof. Mounted on top of this is a Bruker Solar Tracker type A547 (see Fig. 3). It follows the sun and guides the sunlight into the container. The flange and the tracker have to be protected from bad weather such as rain, snow and high wind speed. Therefore a special dome was developed.

2.3.1 The solar tracker dome

The dome for the solar tracker is a crucial part of the system. It has to meet several demands. In the closed state it should be small but still allow the tracker to move into every position. It has to protect the tracker and the flange beneath from rain, snow and hail as well as strong winds and flying debris. In the open state it should allow the tracker an unobstructed 360° view. The mechanism has to be simple and reliable.

Our solution to these demands consists of a frame of aluminum x-profile beams that are covered with aluminum plates. Its z-shaped movement (see Fig. 4) is realized by two arrays of hinges and a moving lever. This lever is powered by a gear motor via a tooth-belt drive.

AMTD
3, 3067–3103, 2010

The middle part (Part B in Fig. 4) was constructed as an open frame. Therefore the area exposed to the wind does not increase during the opening or closing process. This way, even high wind speeds do not inhibit the movement of the dome. This ensures that it can be closed under all conditions. Also note that the upper part of the lid always faces upwards. This way the tracker cannot be harmed by water, dirt or other objects (leafs etc.) that may have collected in the open lid when the dome is closed.

2.3.2 The shutter

A failure of the dome mechanism cannot be ruled out completely. Therefore, an additional shutter was constructed as a backup mechanism to close the container even in case the dome should fail. The shutter also provides additional thermal insulation between the container and the dome. This saves energy and avoids condensation problems when the dome is closed.

The shutter basically works like a drawer and is mounted on the ceiling directly underneath the flange (Fig. 2). Usually it is opened and closed simultaneously with the dome but can be operated independently if necessary. The main part is a polyamide block with a hole on one and a drain on the other side. It slides via four ball bearings on two polished steel rails. The shutter is moved by a spindle-motor and the accurate positioning is realized with two limit switches. In the open position, the hole in the shutter is congruent with the hole in the flange. This way the sun light can travel from the tracker down into the spectrometer.

When the shutter is closed, the drain slides under the hole in the flange and seals the container. In case of a dome failure, rain is collected by the drain and guided into a reservoir.

2.4 Automation

For the automation the system was divided in three autonomous modules. Each of these modules is designed to be as reliable as possible. In case of a malfunction or

AMTD
3, 3067–3103, 2010

a complete failure of a component, the modules bring the system to a defined standby or sleeping status. This way it is very unlikely that the system ends up in an undefined state.

2.4.1 Weather station

The weather station (Fig. 5) is equipped with a number of different sensors to monitor outdoor and indoor conditions (Table 1). Most of the sensors are redundant since their data are either crucial for the measurement process or for the protection of the system against bad weather.

Indoor as well as outdoor temperature and humidity are measured by redundant pairs of sensors. A pyranometer measures global radiation which is useful to determine appropriate measurement conditions without opening the dome. Wind speed is measured by two cup anemometers that were chosen for their reliability. Precipitation is detected by two different approaches: The first sensor works with a light barrier that can detect rain, hail and also other flying objects like insects. The second precipitation sensor detects changes in conductivity when it is hit by rain or snow. This one is also able to detect fine spray.

Highly accurate and stable pressure measurements are essential for the quality of the retrieved mixing ratio profiles (see Eq. 2). However, long-term drift of these sensors is a problem that cannot be avoided easily. To be able to detect and correct such a drift three highly accurate digital Vaisala PTB210 pressure sensors and a special recalibration scheme where chosen.

Figure 6 explains how this recalibration scheme works: Sensors 1 and 2 are used for redundant measurements while sensor number 3 is a calibrated spare. At a regular maintenance visit sensor 3 will replace one of the two used sensors (sensor 1 in this example). Sensor 1 will then be recalibrated and later replace the other sensor – in this example sensor 2 – during the next maintenance visit. This leap-frog calibration scheme allows to detect and compensate any drift of the sensors. One sensor always stays in the system as a reference. This way, a detected drift in one of the sensors

AMTD
3, 3067–3103, 2010

can be corrected and discontinuities in the pressure measurements can be avoided. With this scheme, one should be able to maintain the original ±0.1 hPa accuracy of the sensors over a period of many years.

The precipitation sensors are directly connected to the PLC (see Sect. 2.4.2) to ensure that dome and shutter can be closed as quickly as possible when it starts to rain. All other sensors are connected to a Campbell Scientific CR 1000 data logger. This data logger processes the raw data and makes them available to the Master PC via an ethernet connection (Fig. 7). Details of the weather station can be found in (Zöphel, 2008).

2.4.2 Programmable Logic Controller (PLC)

The Programmable Logic Controller (PLC) is the backbone of the container and one of the most crucial components. Its main target is to bring the container into one of several predefined states depending on external circumstances. It also indicates this status to the Master PC and executes its requests to change this status (Fig. 7). The PLC has full control of the dome and the shutter and controls the power lines of most other components (including the Master PC). The PLC is also connected to different sensors and switches to determinate the status of many components. The communication to the Master PC is established via an RS232 connection. If the Master PC should fail to communicate with the PLC for too long, the PLC will try to restart the Master PC.

The PLC has two operational modes that can be chosen via a selector switch. The automatic mode shows the actual container status on the PLCs main screen (Fig. 8). Colored bullets indicate the status of each component: green stands for “OK”, yellow for “in progress” and red indicates “alert”. More detailed information can be accessed via sub menus. In this mode the PLC accepts commands only via RS232 communication – or in case of an emergency – via direct command input via Ethernet. Every input command is answered by the PLC with a detailed list of the actual status of every input and output channel. Invalid commands are ignored.

AMTD
3, 3067–3103, 2010

The other operation mode – the manual mode – is for manual operation during maintenance. In this mode all parts of the PLC system can be accessed and operated manually through their sub menus. External commands from the Master PC are ignored in this mode.

In case of a power failure the PLC ensures that all components are properly shut down and the dome is closed before the UPS battery runs out. It is also the first system that automatically restarts after such a shutdown. All the other components are afterwards restarted in a defined cascade until the whole system is fully operational again.

2.4.3 Dual PC

For high availability the container is equipped with an industrial 19-inch rack-mount computer system. The chassis includes a redundant power supply, temperature monitoring, and a temperature controlled fan cascade. It hosts two independent Slot-CPUs in the same case: one for the measurement process, communication and data storage (Master PC) and one for the control of the solar tracker (Tracker PC). Passively cooled low-energy CPUs were chosen to avoid a system malfunction due to a fan failure.

The Master PC stores its data on a high-availability RAID system with twelve hard disks. The total usable disk space in the current configuration is 280 GB with four redundant disks and four spare disks. The maximum configurable redundant disk space would be 792 GB with no spares. Disk configurations can be changed while the system is operating (even remotely). The Tracker PC needs very little disk space and runs from a flash memory card.

Master PC

The Master PC is connected to both the PLC and the Tracker PC via RS232. It also communicates with the weather station's data logger via ethernet (Fig. 7). Background of the automation program is a Linux system that stores the weather data and various

AMTD
3, 3067–3103, 2010

container status parameters in a MySQL database. Based on this data the Master PC decides whether the conditions are good enough for a measurement. A positive decision leads to a request to the PLC to bring the system into measurement mode. A negative decision leaves the container in or puts it back to standby mode.

2.5 Communication, data storage and transfer

The container can be accessed remotely in two ways. First, it has a wireless link that can cover up to 2 km to the next available internet access. It also is equipped with a BGAN satellite receiver that provides internet connection almost anywhere in the world. However, the transfer of large amounts of data over the satellite link is very expensive, so this link is intended mostly for remote control. If there is no alternative internet connection, data can also be saved to 72-GB DDS (DAT) tapes which can be mailed easily.

3 First results

3.1 Instrument line shape

For the accurate retrieval of total column values, a good alignment of the FTIR is crucial. The instrument line shape (ILS) retrieved from HCl cell measurements is a useful indicator of the FTIR's alignment (Hase et al., 1999). The performed measurements were analyzed with the Linefit spectrum fitting algorithm (Hase, 2010).

Figures 9 and 10 show the results of an ILS retrieval from HCl cell measurements from August 2009 and February 2010. The modulation efficiency decreased slightly during these six months (Fig. 10). Nevertheless, the maximum loss in modulation efficency is 3%. For comparison other well aligned TCCON intruments reach values for modulation efficency of better then 95%. The phase error for both measurements is well below 0.01 rad which Hase et al. (1999) considered as a good value. A closer look at the ILS (Fig. 9) shows a symmetric line shape for both measurements.

AMTD
3, 3067–3103, 2010

3.2 Column measurements at Jena

In 2009 measurements were taken during the setup of the instrument and the automation of the system. Due to the ongoing construction, the time series is relatively sparse. The site is located at the outskirts of Jena, Germany, at 50.910° N, 11.569° E, 211 m a.s.l.

The acquired data was processed with TCCON standard analysis software GGG. GGG is a suite of software tools developed at Jet Propulsion Laboratory (JPL) to determine the abundances of atmospheric trace gases from infrared solar absorption spectra. This software evolved from the ODS software (Norton and Rinsland, 1991) used for the Version 2 analysis of ATMOS data, but has incorporated many improvements since then. The most complex program in the GGG suite is GFIT, the spectral fitting code. GFIT has been used for the analysis of MkIV spectra (balloon, aircraft, and ground-based), plus the Version 3 analysis of ATMOS shuttle spectra (Irion et al., 2002). Also GFIT has been used for the analysis of spectra from several ground-based FTIR spectrometers (Notholt et al., 1997). In recent years GFIT and has become the standard data analysis tool for TCCON. The number of species retrieved from GFIT and the associated number of analyzed micro windows after TCCON specifications can be found in Table 2.

CO_2 is retrieved in the 6220 cm^{-1} and 6339 cm^{-1} bands, O_2 in the 7885 cm^{-1} band, CH_4 in the 5938 cm^{-1}, 6002 cm^{-1} and 6076 cm^{-1} bands and CO in the 4233 cm^{-1} and 4290 cm^{-1} bands. The dry air column-averaged mole fractions are calculated from the gas columns (Γ), according to

$$f_{CO_2,avg} = \frac{\Gamma_{CO_2}}{\Gamma_{dry\ air}} \quad (1)$$

AMTD
3, 3067–3103, 2010

As mentioned by Washenfelder et al. (2006), there are two methods for calculating the total dry column $\Gamma_{\text{dry air}}$. Both methods have specific advantages and disadvantages:

$$\Gamma_{\text{dry air,P}} = \frac{P_S}{m_{\text{air}} g} - \Gamma_{H_2O} \quad (2)$$

with m_{air} – air mass, P_S – surface pressure, g – gravity constant

$$\Gamma_{\text{dry air,O}_2} = \frac{\Gamma_{O_2}}{0.2095} \quad (3)$$

In general the approach of calculating the total dry column via surface pressure with Eq. (2) is more precise since P_S can be measured very accurately (see Sect. 2.4.1). Using the more noisy retrievals of the O_2 column for the calculation in Eq. (3) will increase the random scatter. Non-perfect measurement conditions (like pointing errors and variation of intensity during the measurement) and systematic errors will affect the O_2 and CO_2 retrievals similarly. Those are eliminated when $\Gamma_{\text{dry air,O}_2}$ is used in Eq. (1).

Figure 12 shows the change with the solar elevation angle of the GFIT averaging kernel for xCO_2 over Jena. These kernels have been determined for the CO_2 6220 cm^{-1} band. The averaging kernel represents the change in the retrieved total column abundance with respect to a perturbation of the true profile at a particular level/altitude.

The diurnal variation of total column xCO_2 over Jena (Fig. 13) illustrates the decrease in atmospheric xCO_2 over the covered period in more detail. It shows also that the decrease of xCO_2 over the day is relatively constant.

In addition, we compared the total column xCO_2 data measured with the Jena FTIR to ground-based in-situ CO_2 measured on the roof the MPI for Biogeochemistry. The in-situ measurements are performed with non-dispersive infrared (NDIR) gas analyzer type LI-COR LI-6262. The diurnal variation of xCO_2 next to the ground is not well represented by the column measurements (Figs. 14 and 15). The large drop of more than 80 ppm in boundary layer CO_2 was not represented in the total column measurements.

AMTD
3, 3067–3103, 2010

This shows that the contribution of the boundary layer to the total column is presumably small. The FTIR measurements after 10:00 a.m. show a relative constant offset compared to the in-situ measurements.

Figure 16 shows the comparison total column xCO_2 daily averages vs. total column values calculated from TM3 inversions (Rödenbeck, 2005). Unfortunately, TM3 result were only available until the end of 2007. To compare them with the FTIR results, the TM3 results were extrapolated to 2009. For this extrapolation, the yearly cycles of 1996 till 2007 were averaged and scaled to the 2007 mean. This reduced the synoptic variability. The mean yearly cycle was then shifted for the annual mean CO_2 growth rate for the years 2008 (1.80 ppm) and 2009 (1.64 ppm) (NOAA/ESRL, 2010) by adding an offset of +3.44 ppm. The red empty boxes represent xCO_2 measured by the FTIR, respectively the daily mean (for day where more then one measurement could be performed). The vertical red lines represent the standard error of the mean value. The FTIR total column xCO_2 values represent the prognosted yearly cycle of 2009 well and are within respectivly close to the 1σ threshold.

4 Conclusions and outlook

This article describes the principal components and the design concept of the MPI-BGC FTIR system. The main design goals were reliability and low maintenance effort for operation at remote sites. This was realized through the interaction of independent subsystems that were kept as simple as possible. Critical components are redundant as much as possible.

During the installation phase at Jena, Germany, the instrument measured column-averaged xCO_2, xCO and xCH_4. Compared to ground-based in-situ CO_2 VMR measurements, the FTIR total column xCO_2 showed an expected offset in the morning which mostly disappeared with the breakup of the nighttime planetary boundary layer. This effect demonstrated the reduced sensitivity of xCO_2 measurements to mixing processes in the planetary boundary layer. Otherwise, the xCO_2 measurements show

AMTD
3, 3067–3103, 2010

a distinct diurnal cycle. The short seasonal cycle measured over Jena during the installation phase corresponded to TM3 simulation results that were extrapolated to 2009 values.

The instrumental line shape of the FTIR was determined from HCl cell measurements. During a period of six months this ILS changed only slightly. From these results one can expect that – once aligned – the instrument will be very stable over long time persiods.

In September/October 2009 the MPI-BGC FTIR system and five other European FTIR stations took part in the IMECC aircraft campaign. The goal of this campaign was to determine a calibration factor between total column values calculated from in-situ aircraft profiles of CO_2, CH_4, and CO and corresponding total column values retrieved from ground-based FTIR. The results from this campaign will be published separately in the near future.

The FTIR will first take part in a test campaign to Wollongong, Australia, from June to September/October 2009. This campaign will provide a rare opportunity of a side-by-side intercomparison of two TCCON-type FTIR instruments on the Southern Hemisphere.

After the campaign, the instrument will be shipped to Ascension Island (7.93° S, 14.37° W) to commence long-term measurements. From this unique location it will provide the first long time series of xCO_2, xCH_4 and other column-averaged greenhouse gases in the Tropical Western Hemisphere. Ascension Island was selected because it frequently receives air masses from the rain forest regions of Africa and occasionally also from South America. Figure 17 shows a one-year footprint for the total column measurements expected from Ascension Island. Other groups will provide very valuable in-situ surface measurements of CO_2 and CH_4 from the same site.

AMTD
3, 3067–3103, 2010

Acknowledgements. We would like to thank many people who have contributed to this project: the mechanical and electronic workshop of the MPI-BGC for their support, Frank Hase (IMK-FZK) for his help with the ILS analysis, all members of the Total Carbon Column Observation Network (TCCON) for their fruitful colaboration, Christian Rödenbeck for his TM3 data, the Max Planck Society for funding this instrument.

The service charges for this open access publication have been covered by the Max Planck Society.

References

Dufour, E., Bréon, F.-M., and Peylin, P.: CO_2 column averaged mixing ratio from inversion of ground-based solar spectra, J. Geophys. Res., 109, D09304, doi:10.1029/2003JD004469, 2004. 3069

Gerbig, C., Körner, S., and Lin, J. C.: Vertical mixing in atmospheric tracer transport models: error characterization and propagation, Atmos. Chem. Phys., 8, 591–602, doi:10.5194/acp-8-591-2008, 2008. 3069

GLOBALVIEW-CO2: Cooperative Atmospheric Data Integration Project – Carbon Dioxide. CD-ROM, NOAA ESRL, Boulder, Colorado, ftp://ftp.cmdl.noaa.gov/ccg/co2/GLOBALVIEW, 2009. 3068

Gloor, M., Fan, S.-M., Pacala, S., and Sarmiento, J.: Optimal sampling of the atmosphere for purpose of inverse modeling: a model study, Glob. Biogeochem. Cy., 14, 407–428, doi:10.1029/1999GB900052, 2000. 3069

Gurney, K. R., Law, R. M., Denning, A. S., Rayner, P. J., Baker, D., Bousquet, P., Bruhwiler, L., Chen, Y.-H., Ciais, P., Fan, S., Fung, I. Y., Gloor, M., Heimann, M., Higuchi, K., John, J., Maki, T., Maksyutov, S., Masarie, K., Peylin, P., Prather, M., Pak, B. C., Randerson, J., Sarmiento, J., Taguchi, S., Takahashi, T., and Yuen, C.-W.: Towards robust regional estimates of CO_2 sources and sinks using atmospheric transport models, Nature, 415, 626–630, doi:10.1038/415626a, 2002. 3068

Hase, F.: Linefit spectrum fitting algorithm, http://www-imk.fzk.de/asf/ftir/linefit.htm, 2010. 3077

Hase, F., Blumenstock, T., and Paton-Walsh, C.: Analysis of the instrumental line shape of high-resolution Fourier Transform IR spectrometers with gas cell measurements and new

AMTD

3, 3067–3103, 2010

retrieval software, Appl. Optics, 38, 3417–3422, doi:10.1364/AO.38.003417, 1999. 3072, 3077

Irion, F. W., Gunson, M. R., Toon, G. C., Chang, A. Y., Eldering, A., Mahieu, E., Manney, G. L., Michelsen, H. A., Moyer, E. J., Newchurch, M. J., Osterman, G. B., Rinsland, C. P., Salawitch, R. J., Sen, B., Yung, Y. L., and Zander, R.: Atmospheric Trace Molecule Spectroscopy (ATMOS) experiment version 3 data retrievals, Appl. Optics, 41, 6968–6979, doi:10.1364/AO.41.006968, 2002. 3078

NOAA/ESRL: Dr. Pieter Tans, NOAA/ESRL, www.esrl.noaa.gov/gmd/ccgg/trends, 2010. 3080

Norton, R. H. and Rinsland, C. P.: ATMOS data processing and science analysis methods, Appl. Optics, 30, 389–400, doi:10.1364/AO.30.000389, 1991. 3078

Notholt, J., Toon, G., Stordal, F., Solberg, S., Schmidbauer, N., Becker, E., Meier, A., and Sen, B.: Seasonal variations of atmospheric trace gases in the high Arctic at 79° N, J. Geophys. Res., 102, 12855–12861, doi:10.1029/97JD00337, 1997. 3078

Petersen, A. K., Warneke, T., Frankenberg, C., Bergamaschi, P., Gerbig, C., Notholt, J., Buchwitz, M., Schneising, O., and Schrems, O.: First ground-based FTIR-observations of methane in the tropics, Atmos. Chem. Phys. Discuss., 10, 2303–2320, doi:10.5194/acpd-10-2303-2010, 2010. 3069

Rayner, P. J. and O'Brien, D. M.: The utility of remotely sensed CO_2 concentration data in surface source inversions, Geophys. Res. Lett., 28, 175–178, doi:10.1029/2000GL011912, 2001. 3069

Rayner, P. J., Enting, I. G., Francey, R. J., and Langenfelds, R.: Reconstructing the recent carbon cycle from atmospheric CO_2, $\delta^{13}C$ and O_2/N_2 observations, Tellus B, 51, 213–232, doi:10.1034/j.1600-0889.1999.t01-1-00008.x, 1999. 3068

Rödenbeck, C.: Estimating CO_2 sources and sinks from atmospheric mixing ratio measurements using a global inversion of atmospheric transport, Tech. Rep. 6, Max Planck Institute for Biogeochemistry, Jena, Germany, http://www.bgc-jena.mpg.de/mpg/websiteBiogeochemie/Publikationen/Technical_Reports/tech_report6.pdf, 2005. 3080, 3103

Tans, P. P., Fung, I. Y., and Takahashi, T.: Observational constraints on the global atmospheric CO_2 budget, Science, 247, 1431–1438, doi:10.1126/science.247.4949.1431, 1990. 3068

Toon, G., Blavier, J.-F., Washenfelder, R., Wunch, D., Keppel-Aleks, G., Wennberg, P., Connor, B., Sherlock, V., Griffith, D., Deutscher, N., and Notholt, J.: Total Column Carbon Observing Network (TCCON), in: Fourier Transform Spectroscopy, OSA Technical Digest (CD), p. paper JMA3, Optical Society of America, Vancouver, Canada, http://www.opticsinfobase.

AMTD
3, 3067–3103, 2010

org/abstract.cfm?uri=FTS-2009-JMA3, 2009. 3069

Warneke, T., Yang, Z., Olsen, S., Körner, S., Notholt, J., Toon, G. C., Velazco, V., Schulz, A., and Schrems, O.: Seasonal and latitudinal variations of column averaged volume-mixing ratios of atmospheric CO_2, Geophys. Res. Lett., 32, L03808, doi:10.1029/2004GL021597, 2005. 3069

Washenfelder, R. A., Toon, G. C., Blavier, J.-F., Yang, Z., Allen, N. T., Wennberg, P. O., Vay, S. A., Matross, D. M., and Daube, B. C.: Carbon dioxide column abundances at the Wisconsin Tall Tower site, J. Geophys. Res., 111, D22305, doi:10.1029/2006JD007154, 2006. 3069, 3071, 3079

Yang, Z., Toon, G. C., Margolis, J. S., and Wennberg, P. O.: Atmospheric CO_2 retrieved from ground-based IR solar spectra, Geophys. Res. Lett., 29, 1339, doi:10.1029/2001GL014537, 2002. 3069

Yokota, T., Yoshida, Y., Eguchi, N., Ota, Y., Tanaka, T., Watanabe, H., and Maksyutov, S.: Global concentrations of CO_2 and CH_4 retrieved from GOSAT: first preliminary results, SOLA, 5, 160–163, doi:10.2151/sola.2009-041, 2009. 3069

Zöphel, H.: Test and installation of an automatic weather station to provide ground-based FTIR measurements for TCCON, Master's thesis, University of Applied Sciences, Jena, Germany, http://www.bgc-jena.mpg.de/bgc-systems/dissertations/diploma/diploma_hendrik_zoephel-reduced.pdf, 2008. 3075

AMTD
3, 3067–3103, 2010

Table 1. Weather station equipment.

Sensor	Position
Temperature	2 outdoor, 2 indoor, 2 in the FTIR
Humidity	2 outdoor, 2 indoor
Global radiation	1 outdoor
Precipitaion	2 outdoor
Wind speed	2 outdoor
Ambient pressure	2 outdoor

AMTD
3, 3067–3103, 2010

Table 2. Table of species retrieved from GFIT and the associated number of analyzed micro windows according to TCCON specifications.

Species	Micro Windows	Standard output
CH_4	3	yes
CO	2	yes
CO_2	2	yes
HF	1	yes
HCl	16	no
HDO	4	yes
H_2O	9	yes
N_2O	2	yes
O_2	1	no

AMTD
3, 3067–3103, 2010

Fig. 1. Picture of the MPI-BGC FTIR container at its preliminary location close to the MPI-BGC in Jena.

AMTD
3, 3067–3103, 2010

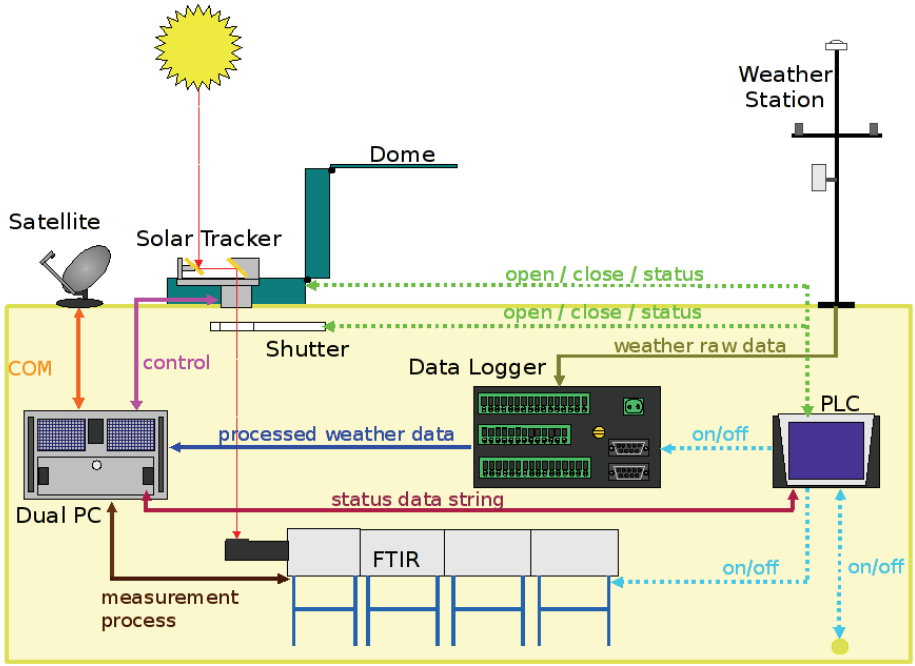

Fig. 2. Schematic overview of the MPI-BGC FTIR system. It illustrates all major parts of the system. The communication flow between the individual components is indicated by arrows.

AMTD
3, 3067–3103, 2010

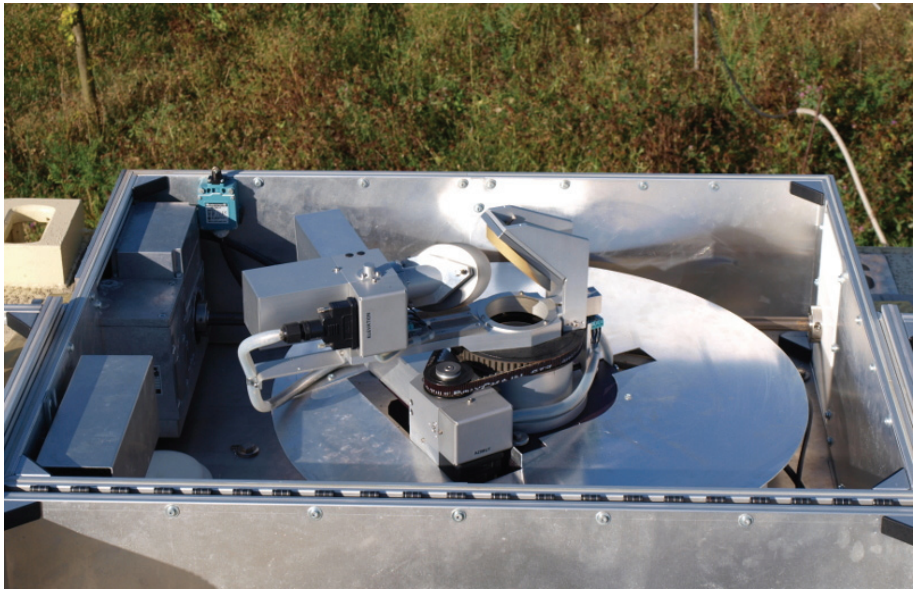

Fig. 3. The Bruker Solar Tracker type A547 mounted in the custom made dome (shown in open state).

AMTD
3, 3067–3103, 2010

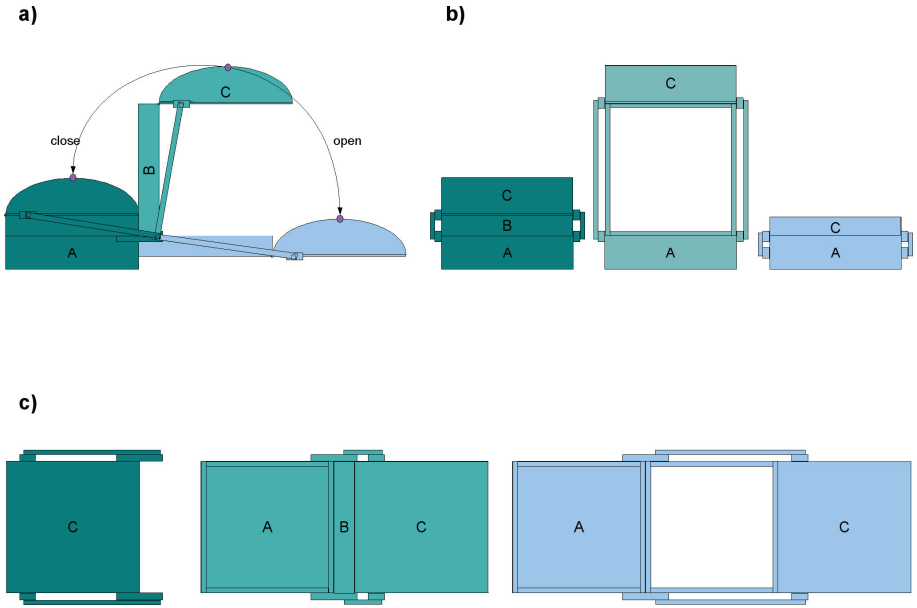

Fig. 4. Schematic overview of the BGC-FTIR Solar Tracker Dome in side **(a)**, front **(b)** and top view **(c)**. It consists of a frame of aluminum *x*-profile beams that are covered with aluminum plates. Its *z*-shaped movement is realized by two arrays of hinges and a moving lever. The middle part (Part B) is an open frame. The upper part (Part C) of the lid always faces upwards.

AMTD
3, 3067–3103, 2010

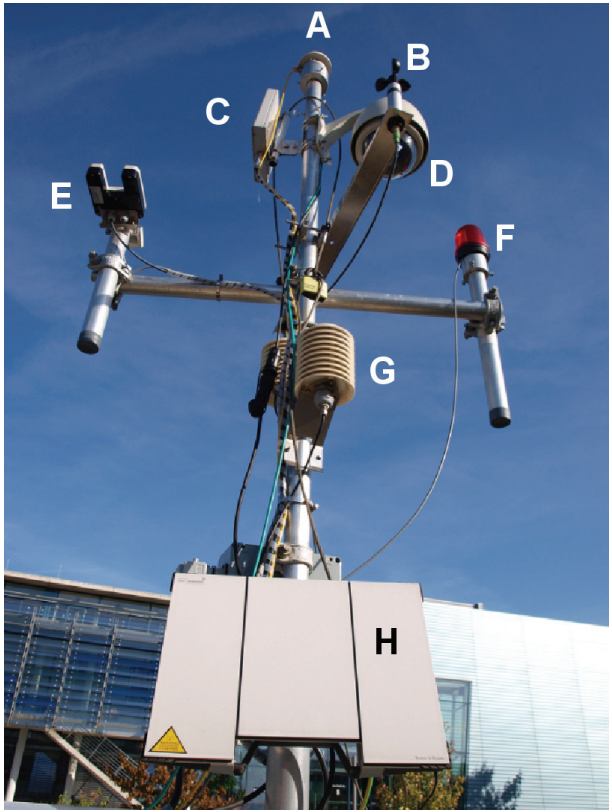

Fig. 5. The weather station mounted on top of the FTIR container. It measures temperature and humidity with two sensors (G). Wind speed is measured by two cup anemometers (B). It is also equipped with two different precipitaion detectors (E). On the very top, global radiation is measured by a pyranometer (A). The pole of the weather station also hosts two antennas for communication: a wireless LAN link (B) and a BGAN satellite receiver (H). Also an outdoor camera (D) and a signal LED (F) are mounted on the pole.

AMTD
3, 3067–3103, 2010

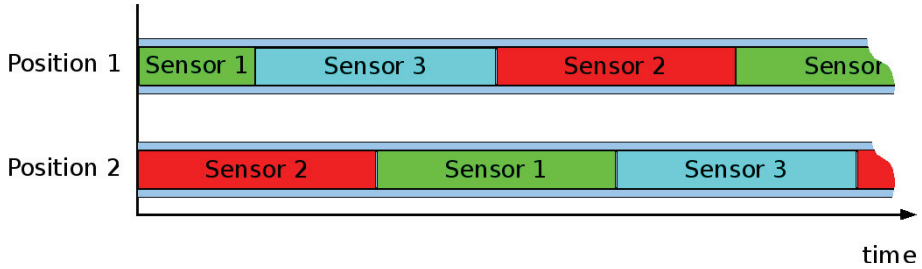

Fig. 6. Pressure sensor recalibration scheme. Sensors 1 and 2 are used for redundant measurements while sensor number 3 is a calibrated spare that replaces one of the two used sensors (e.g. sensor 1) at the next maintenance after aproximately 6 months. Sensor 1 will then be recalibrated and later replace sensor 2.

AMTD
3, 3067–3103, 2010

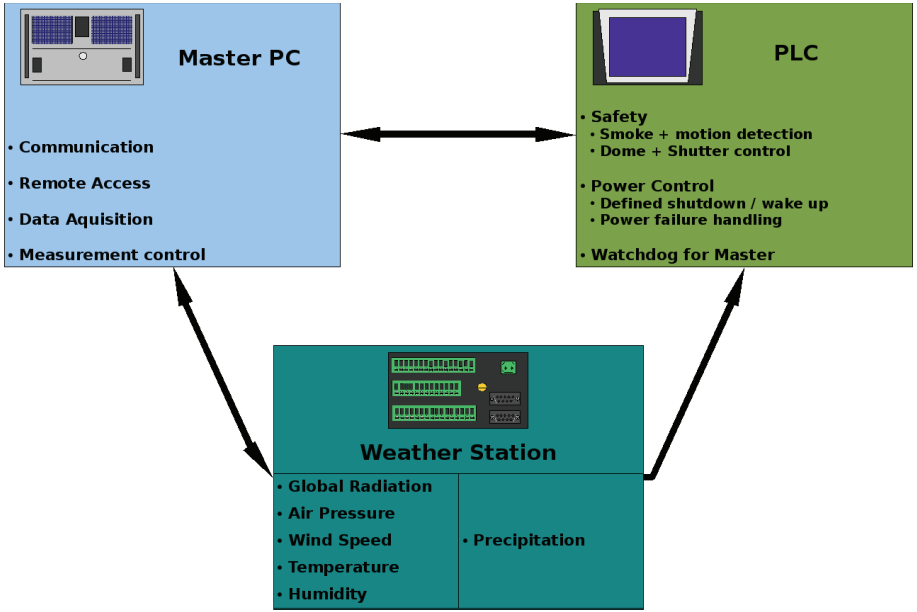

Fig. 7. Schematic overview of the communication. The three major parts of the FTIR system are autonomous systems. They communicate over a serial and an ethernet connection, repectively.

AMTD
3, 3067–3103, 2010

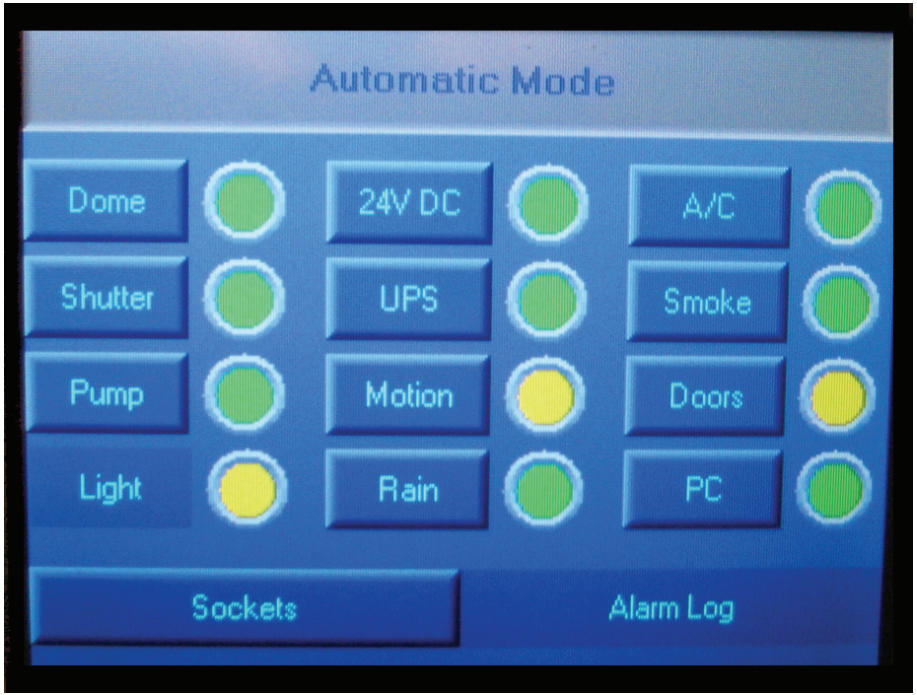

Fig. 8. PLC control panel showing the PLC operating in automatic mode. It shows the actual container status, the colored bullets indicate status of each component – whereas green stands for "OK", yellow for "in progress" and red indicates "alert". Detailed information can be accessed via the sub menus.

AMTD
3, 3067–3103, 2010

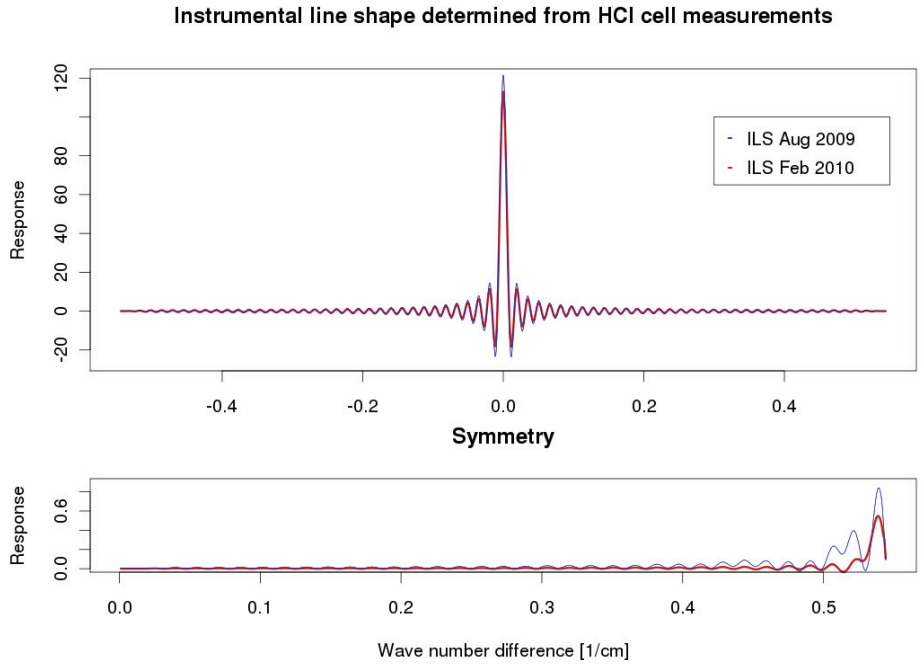

Fig. 9. Comparison of the instrument line shape of the Jena BRUKER IFS125HR in August 2009 and February 2010. Both measurements show a symmetric ILS.

AMTD
3, 3067–3103, 2010

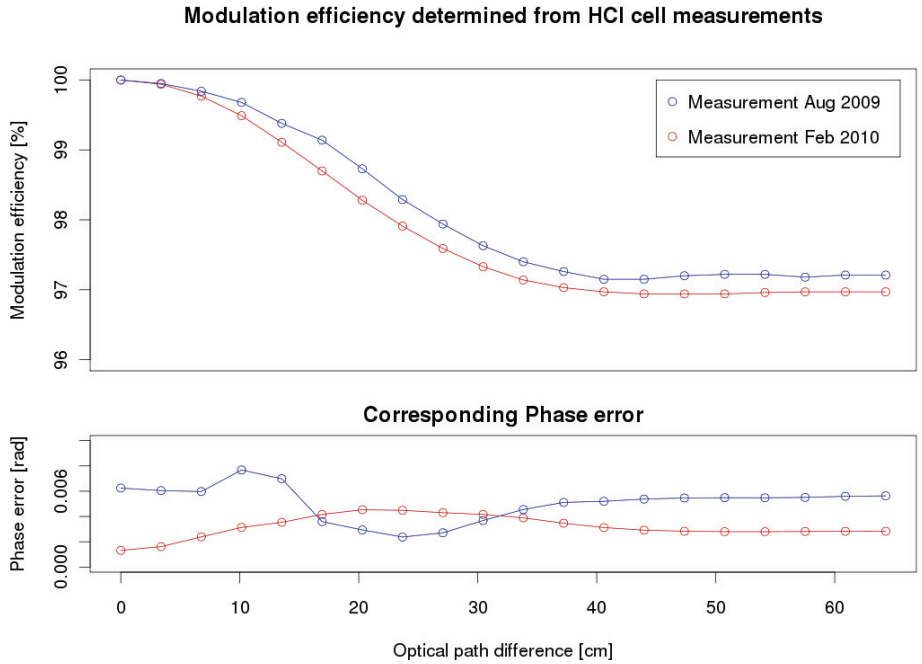

Fig. 10. Changes in the modulation efficiency and phase error of the Jena BRUKER IFS125HR from August 2009 to February 2010.

AMTD
3, 3067–3103, 2010

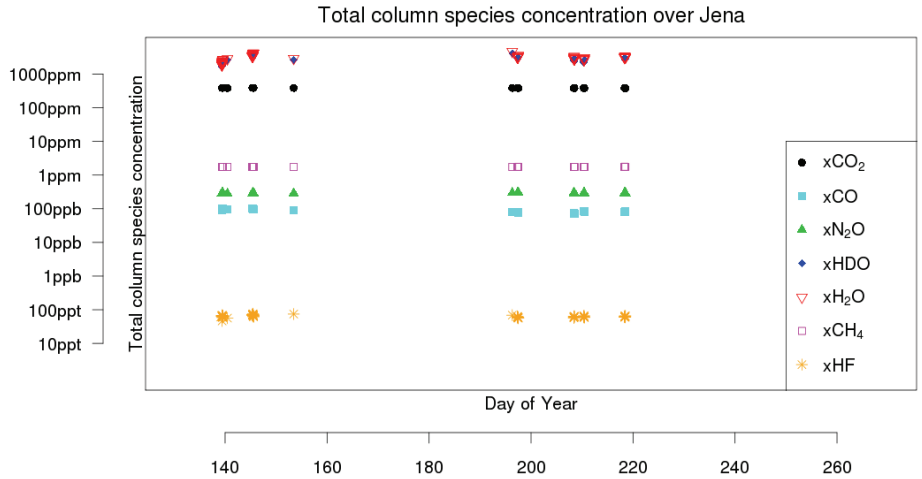

Fig. 11. Standard TCCON anaysis of measurements taken with Jena FTS 2009.

AMTD
3, 3067–3103, 2010

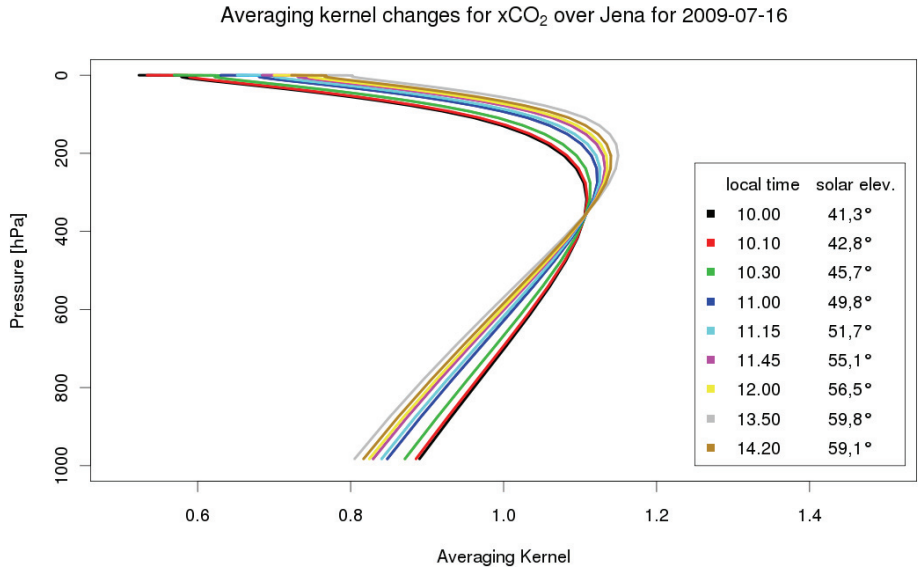

Fig. 12. Changes of the GFIT averaging kernel for xCO_2 over Jena for the measurements performed on 16 July 2009. These kernels have been determined for the CO_2 6220 cm^{-1} band. The averaging kernel is changing with the solar elevation angle.

AMTD
3, 3067–3103, 2010

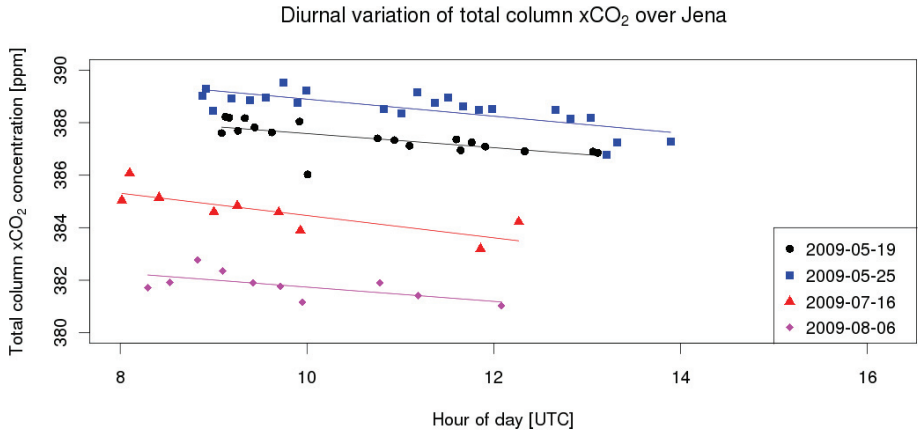

Fig. 13. Diurnal variation of total column xCO_2 over Jena shown on selected days. The decrease of xCO_2 over the day was relatively constant.

AMTD
3, 3067–3103, 2010

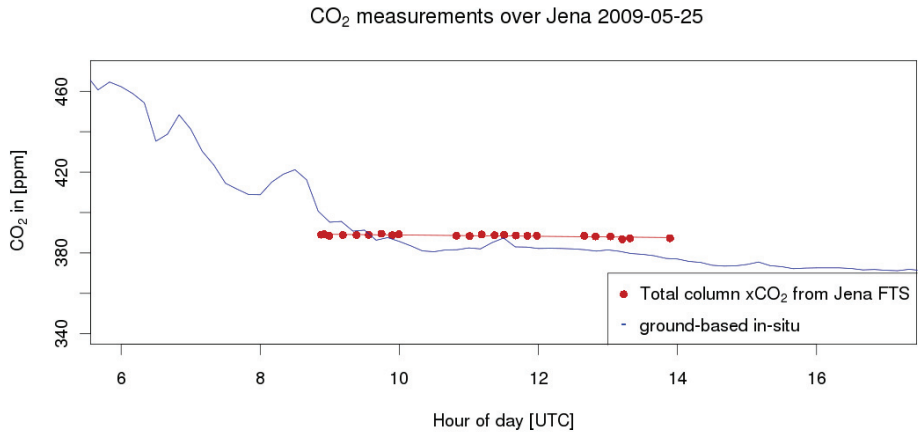

Fig. 14. Diurnal variation of ground-based in-situ CO_2 and total column xCO_2 over Jena. The gaps in the time series are due to clouds.

AMTD
3, 3067–3103, 2010

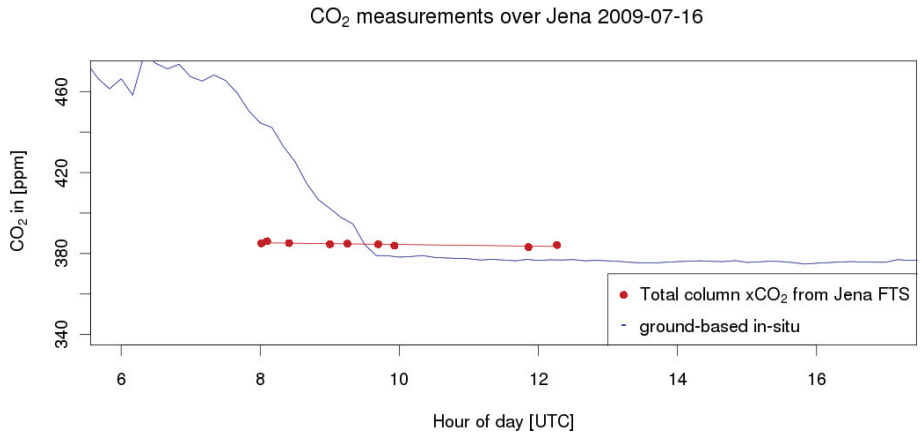

Fig. 15. Diurnal variation of ground-based in-situ CO_2 and total column xCO_2 over Jena. The gaps in the time series are due to clouds.

AMTD
3, 3067–3103, 2010

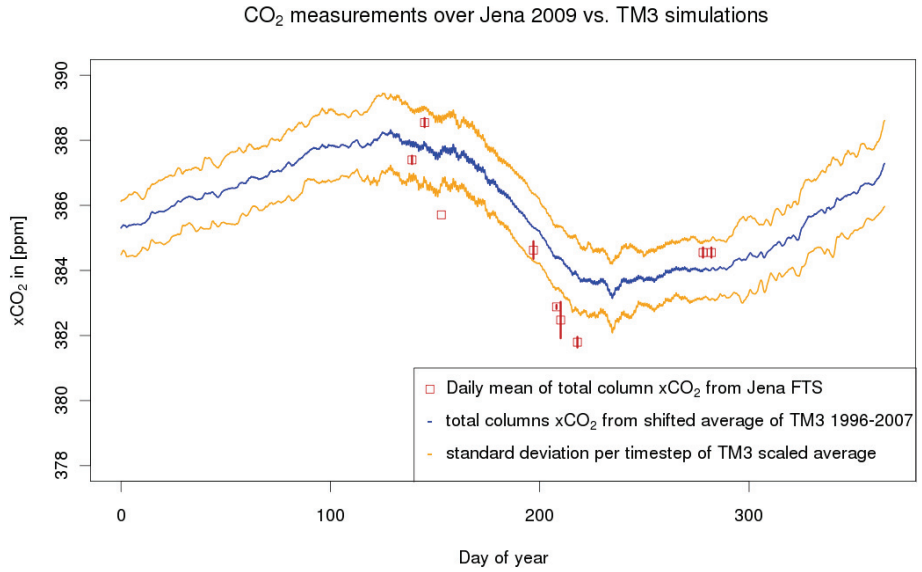

Fig. 16. Total column xCO_2 measurements over Jena vs. extrapolated TM3 results for 2009. Empty red boxes represent individual xCO_2 measurements from the FTIR. Red boxes with vertical lines represent daily mean values of xCO_2 with error bars (vertical lines).

AMTD
3, 3067–3103, 2010

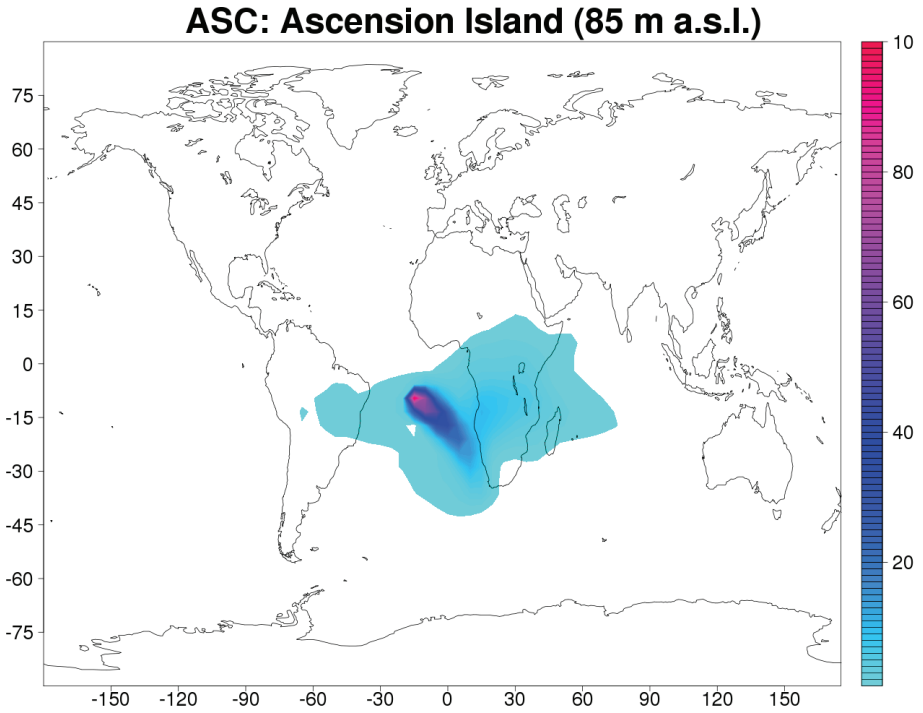

Fig. 17. Footprint analysis for a total-column instrument on Ascension Island. The coloured values represent the relative contribution to the total column for different surface regions in arbitrary units that have been normalized to 100 at the peak value. The footprint was produced using the TM3 adjoint by Rödenbeck (2005) at a horizontal resolution of 5°×3.75° (fine grid). Individual runs for each month of 2006 were integrated to provide this full-year footprint.

AMTD
3, 3067–3103, 2010